THE JOURNAL OF PHYSICAL CHEMISTRY B
A JOURNAL OF THE AMERICAN CHEMICAL SOCIETY

pubs.acs.org/JPCB

Article

Prolonged Association between Water Molecules under Hydrophobic Nanoconfinement

Rui Zhang, Diego Troya,* and Louis A. Madsen*

Cite This: *J. Phys. Chem. B* 2021, 125, 13767−13777

Read Online

ACCESS | Metrics & More | Article Recommendations | Supporting Information

ABSTRACT: We present an investigation of the dynamics of water confined among rigid carbon rods and between parallel graphene sheets with molecular dynamics simulations. Diffusion coefficients, activation energy of diffusion, and residence-time correlation functions as a function of confinement geometry reveal a retardation of water dynamics under hydrophobic confinement compared to bulk water. In fact, water under various confinements possesses longer associations with its neighbors and exhibits diffusion dynamics characteristic of a lower temperature. Analysis of the residence-time correlation functions reveals long and short residence times, which we relate to the diffusion coefficient and activation energy of diffusion, respectively. Additional investigations reveal how the level of confining surface hydrophobicity affects water dynamics, further broadening our understanding of water diffusion inside diverse media. Overall, this study sheds light on the physical origin of retarded water dynamics under hydrophobic confinement and the close relationship between residence times and diffusion behavior.

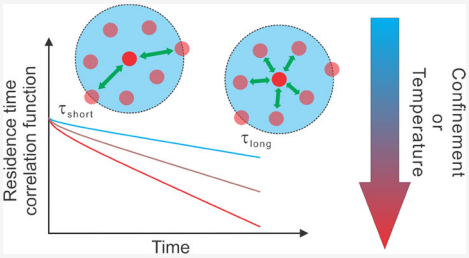

INTRODUCTION

Water is the most abundant molecule on the surface of Earth. While the majority of water is present in the form of liquid bulk water, nanoconfinement of water molecules holds rich implications for a variety of fields such as inorganic porous materials,[1−3] water desalination,[4,5] and biological systems.[6−8] Confining water into structures on the nanometer lengthscale has a sharp effect on several of its properties compared to those of bulk water.[9,10] The physical properties of confined water such as phase transitions,[5,10,11] density,[12,13] energy landscape,[12] structural features,[5,14−16] and dynamics[12,17] have received intense study in the past few decades. Specifically, the dynamics of confined water impacts a wide range of interests including transport in biological systems,[12,18,19] flow through inorganic materials such as nanoporous silica and cement,[20−24] and transport in polymer membranes such as ion-exchange and reverse-osmosis membranes.[25−29]

The dynamics of confined water depends on the hydrophilicity/hydrophobicity of the confining medium. On the one hand, retarded water dynamics usually dominates under hydrophilic confinement.[21,30−32] On the other hand, studies of the motions of water molecules confined inside a hydrophobic environment have provided mixed results. Majumder et al.[33] reported enhanced water flow through carbon nanotubes (CNTs) of 7 nm in diameter. Holt et al.[17] reported measurements of water motion through 2 nm CNT composite membranes and also observed a flow enhancement as compared to bulk water. Zaragoza et al.[13] simulated the diffusion of water inside CNTs and between graphene walls, with both tube diameter and wall separation above 2 nm, and found enhanced water diffusion in both structures. Layfield and Troya[34] conducted simulations of water confined between hydrophobic alkanethiol monolayers and observed enhanced diffusion of water near the hydrophobic surface. In other publications, retarded water dynamics dominates under hydrophobic confinement. Choudhury et al.[35,36] simulated water confined between hydrophobic solutes and observed retarded translational and rotational dynamics of water. Liu et al.[37] and Farimani and Aluru[38] reported diffusion coefficients of water confined in CNTs with varying diameters and observed retarded water dynamics when the tube diameter was below 2 nm. In previous work by our group,[39] we investigated the activation energy of diffusion (E_a) of confined liquid water with both experimental and computational techniques and concluded that nanoconfinement prompts the formation of partially structured water as well as an elevation of E_a.

Retarded water dynamics under hydrophobic confinement, which usually happens under a relatively small confinement size (smaller than 2 nm), has not received sufficient justification. Understanding impeded water motion under hydrophobic confinement provides new fundamental understanding and illuminates new directions toward practical applications of nanoporous materials. In this work, we aim to address the origin of slowed water dynamics under hydro-

Received: August 1, 2021
Revised: November 26, 2021
Published: December 13, 2021

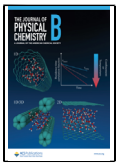

https://doi.org/10.1021/acs.jpcb.1c06810
J. Phys. Chem. B 2021, 125, 13767−13777

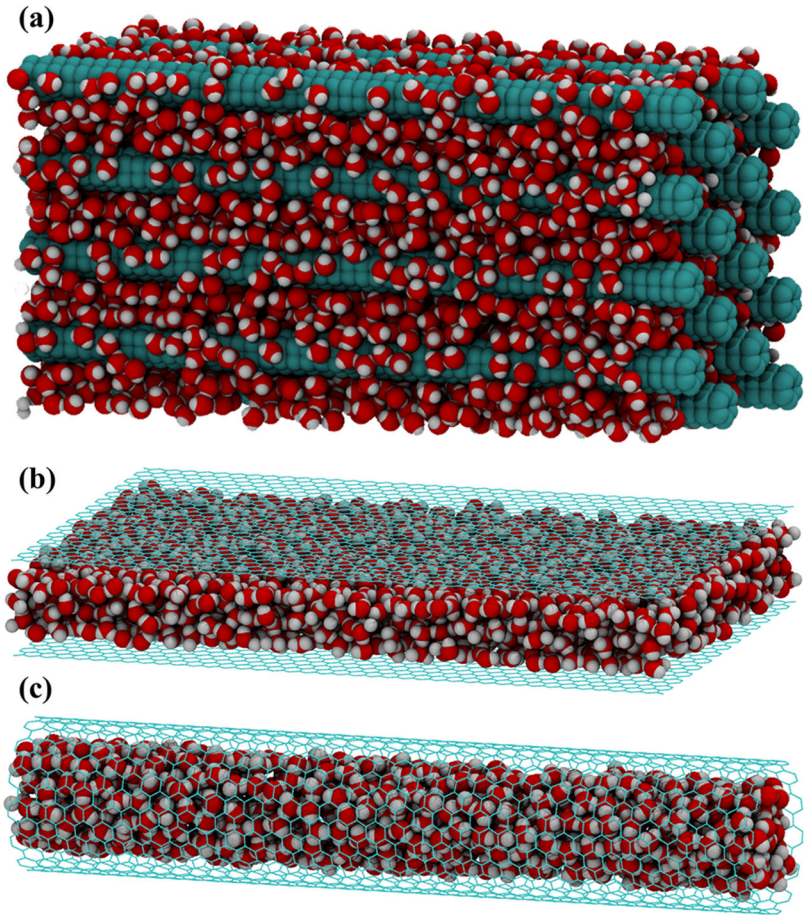

Figure 1. Schematic representations of the simulation models involved in this work. Panel (a) represents the rigid-rod model. The rod−rod distance in the figure is 1.2 nm. Sixteen 16.8 nm-long rigid rods are present in a hexagonal packing pattern in all the rigid-rod simulations. Panel (b) represents the parallel-sheet model. The layer-to-layer distance shown in the figure is 1 nm. The graphene layers are 16 nm in length and 6 nm in width. Panel (c) is the CNT model adapted from previous work.[39] Water reservoirs are used in all three models (see the text). Alternate views of these models are available in Figure S1.

phobic confinement. We describe a remarkable connection between the effect of hydrophobic confinement and temperature: in terms of dynamics, water molecules under hydrophobic confinement behave as if they are at lower temperatures. As far as we know, there is no recognition of whether hydrophobic confinement lowers the effective temperature of water molecules, nor is there qualitative justification of the connections between the effect of hydrophobic confinement and the effect of lowering the actual temperature.

Inspired by previous studies on the dynamics of confined water and supercooled water,[40−43] we quantify the water dynamics under nanoconfinement and with changing temperature by calculating the residence time of water around water. This residence time evaluates the timescale of associations between neighboring molecules. The simulation geometries we investigated are inspired by the structures of actual nanoporous materials, including nanochannels in ionomer membranes[44] and nanoporous silica,[20] the lamellar structure of block copolymers[45] or minerals such as tungsten oxide,[46] and assemblies formed by rigid-rod polymer backbones.[47,48] We observe an increase in the residence time of water around water either when lowering the temperature or when decreasing the confinement size under various confinement geometries, including parallel graphene sheets, parallel rigid rods, and CNTs. In all cases, we observe a clear relation between the translational dynamics/energetics (diffusion coefficients and activation energies of diffusion) and the residence time of water around water. These results emphasize the importance of the residence time as a useful tool to study condensed-phase dynamics and to shed light on the physical origin of retarded water motion under hydrophobic confinement.

METHODS

Simulation Details. We performed all molecular dynamics simulations using the GROMACS 5.0.5 package.[49−51] Figure 1 provides schematics of the simulation models used in this work. Figure 1a is the rigid-rod model. In this model, we place parallel rigid carbon rods in a hexagonal pattern. Each rod consists of 80 stacked carbon-atom rings with six atoms per ring. The distance between the adjacent ring layers is 0.21 nm, providing a total rod length of 16.8 nm, and the distance between the adjacent carbon atoms in each ring is 0.173 nm. We vary the distance between the carbon rods to give different confinement sizes for the solvating water. The rod−rod distances (taken from the center of the rods) range from 1.2 to 2.8 nm. Two water reservoirs are present at each end of the rods, with the total number of water molecules ranging from 11,000 to 42,000 depending on the overall volume of the system. Figure 1b illustrates the parallel-sheet model. This

https://doi.org/10.1021/acs.jpcb.1c06810
J. Phys. Chem. B 2021, 125, 13767−13777

model consists of two graphene sheets, which are 16 nm long and 6 nm wide. We obtain different confinement sizes in this model by varying the layer-to-layer distance from 0.7 to 1.8 nm. We immerse the parallel sheets in a water reservoir whose size is 4 nm × 8 nm × 18 nm. The total number of water molecules in the parallel-sheet model is 16,000. Figure 1c represents the CNT model, which we adapt from our previous publication.[39] The length of the nanotube is 20 nm, and its diameter ranges from 1.4 to 3.2 nm. Water reservoirs are present on both ends of the CNTs, and the total number of molecules in the CNT model ranges from 4000 to 8000. We use SPC/E water[52] in these models for most of the production runs. Nonetheless, the results with TIP4P/2005 water[53] are also presented for a few representative models (included in the Supporting Information).

The simulation systems are periodic in all three directions. We immobilize the confinement structure (rods, sheets, and CNT) using position restraints and assign a large mass (1×10^{20} amu) to each carbon atom. The cut-off distance for Lennard-Jones interactions is 1.2 nm, with the interactions between carbon atoms switched off. We apply particle-mesh Ewald summations to calculate the long-range electrostatic interactions. The force field parameters for carbon atoms are adapted from our previous publication.[39] The equations of motion are solved with a 1 fs timestep, and the calculation of diffusion coefficients employs coordinates recorded each 1 ps. We equilibrate all systems with at least 1 ns NPT simulations followed by multiple 4−8 ns NVT production runs.

Calculated Quantities. We calculate the mean squared displacement (MSD) and diffusion coefficient (D)[54] from NVT simulations using eq 1:

$$D = \frac{\langle |r(t_0 + t) - r(t_0)|^2 \rangle}{2nt} \tag{1}$$

Here, t is the time of diffusion, $r(t)$ is the atomic coordinates at time t, and n is the dimension factor (n equals 1 in the CNT model, 2 in the parallel-sheet model, and 3 in the rigid-rod model). In all models, we calculate the MSD of only water molecules moving within the confined region and ignore the water molecules in the reservoirs. The time interval to calculate the MSD reaches 4 ns, and the diffusion coefficients are extracted from a linear region of MSD vs t plots.

To obtain activation energies of diffusion, we run simulations from 300 to 340 K at 10 K intervals. The activation energy is then obtained from the diffusion coefficients at each temperature following an Arrhenius representation

$$\ln D = \ln D_0 - \frac{E_a}{RT} \tag{2}$$

where D is the diffusion coefficient, D_0 is the pre-exponential factor, E_a is the activation energy of diffusion, R is the gas constant, and T is the temperature.

To calculate the residence time of water, we adapt from the literature the residence-time correlation function $S(t)$[55]

$$S(t) = \langle h(t)h(0) \rangle / \langle h \rangle \tag{3}$$

where $h(t)$ is unity if two water molecules are located within a certain cut-off distance at time 0 and remain continuously in that region through time t; otherwise, $h(t)$ equals 0. We evaluate $\langle h(t)h(0) \rangle$ by taking 1000 different starting points throughout the simulations and averaging over the number of starting points. $\langle h \rangle$ is a normalization factor such that $S(0)$ provides the average number of water molecules around a central molecule within the cut-off distance, which is around 4 for both bulk and confined water. The correlation function $S(t)$ evaluates the timescale of water molecules continuously within the cut-off distance of the target molecule and has been used to quantify the residence time of water molecules around each other[42,56−58] and the timescale for ionic association in solution.[59,60] In the present study, we set the cut-off distance for water association to 0.33 nm (between oxygen atoms) based on the location of the first solvation shell of bulk water. Nevertheless, we discuss the effect of using alternative cut-off distances in Figure S7.

Additionally, we use $S(t)$ to evaluate the associations between water molecules and the hydrophobic rigid rods. Our calculations reveal that the $S(t)$ time correlation function of this work can be well fit with a double exponential decay

$$S(t) = Ae^{-t/\tau_s} + Be^{-t/\tau_l} \tag{4}$$

where A and B are the amplitude fitting parameters and τ_s and τ_l stand for short and long residence times, respectively.[58] This fitting model has been used in several previous studies.[42,58,61] In the stepwise calculation of $S(t)$, the length of the chosen time interval affects the decay time. The correlation function $S(t)$ will fail to capture certain association/dissociation events if the time interval is too long but is computationally intensive if the time step is too short. After trials on different time intervals (see more details in Figure S12), we were able to balance the computational cost and accuracy by evaluating $S(t)$ along the 20−80 ps trajectories with a time interval of 10 fs.

RESULTS AND DISCUSSION

Diffusion Anisotropy and Retarded Water Dynamics in the Rigid-Rod Model. In the rigid-rod model (Figure 1a), we calculated both the diffusion coefficient parallel to the axial direction of the rods (referred to as $D_{\parallel}$) and the diffusion coefficient in the perpendicular plane ($D_{\perp}$). Figure 2 shows the temperature dependence of $D_{\parallel}$ and $D_{\perp}$ as well as the average diffusion coefficient $D_{average}$ for simulations with various rod−rod distances. Note that $D_{\perp}$ is a two-dimensional diffusion coefficient and therefore has a larger contribution to $D_{average}$. In all cases, $D_{\parallel}$ is larger than $D_{\perp}$, which is expected considering that the rods are physically restricting the diffusive motions perpendicular to them. This diffusion anisotropy becomes more prominent with shorter rod−rod distance. Remarkably, the activation energies obtained from the temperature dependence of $D_{\parallel}$ and $D_{\perp}$ are the same, even if the diffusion coefficients are different, which agrees with our conclusion in prior work that the activation energy of diffusion arises from local intermolecular (sub-nm) interactions and is not sensitive to longer range structural features.[25,26,39]

Figure 2c,d presents the $D_{average}$ and the E_a obtained from $D_{average}$ as a function of rod−rod distance. We observe retarded water dynamics at all rod−rod distances as $D_{average}$ is lower than the bulk water diffusion coefficient (dashed lines). The slowdown of water molecules becomes more significant as the confinement size decreases. One apparent reason for the decrease of diffusion coefficients is the physical restrictions from the rigid rods. However, the increase of E_a with decreasing rod−rod distances reveals that the retarded water dynamics originates from not only the tortuous pathways of diffusion but also the increased energy barriers for diffusion.

https://doi.org/10.1021/acs.jpcb.1c06810
J. Phys. Chem. B 2021, 125, 13767−13777

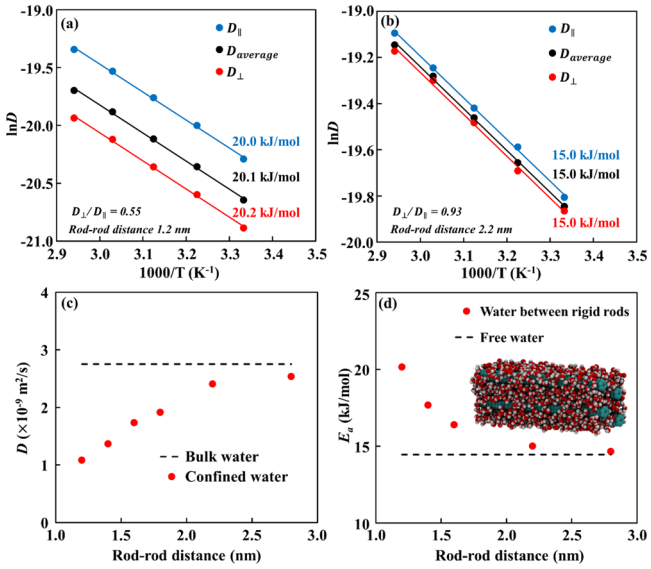

Figure 2. Anisotropic diffusion in the rigid-rod model and change of D and E_a with rod−rod distance. Panels (a, b) show variable-temperature diffusion coefficients at rod−rod distances of 1.2 and 2.2 nm, respectively. The temperature ranges from 300 to 340 K with a 10 K interval. The difference between $D_\parallel$ and $D_\perp$ decreases as the rod−rod distance increases. The activation energies labeling the Arrhenius plots are insensitive to the diffusion direction. Panels (c, d) respectively show the evolution of $D_{average}$ and E_a with rod−rod distance. With decreasing confinement size, $D_{average}$ decreases while E_a increases, suggesting retarded water dynamics in tightly confined media.

The trend of E_a vs confinement size is consistent in all the confining geometries, as E_a increases with decreasing confinement sizes in all models (Figure S4). Interestingly, we observe a more gradual increase of E_a in the rigid-rod model compared to the much sharper increase of E_a when decreasing the nanotube radius in the CNT model. In addition, while partially ordered water with very low diffusion coefficients exists for the narrower nanotubes, highly ordered water is absent in all the rigid-rod models examined. Nonetheless, the elevation of E_a with decreasing confinement size is common to all three simulation models. In this work, we investigate the origin of the increase of E_a with decreasing confinement size in an attempt to understand more deeply the observed retarded water dynamics under hydrophobic confinement.

Parallels between Confinement and Temperature in the Rigid-Rod Model. Figure 3a shows the temperature dependence of all diffusion coefficients in the rigid-rod model at varying rod−rod distance. In Figure 3b, we artificially offset the temperatures of the rigid-rod model diffusion coefficients to make them match the value of bulk water. Remarkably, most of the data points fit very well after the offset. We plot the offset in terms of reciprocal temperature δ_{rt} vs rod−rod distance, porosity, and water's surface-to-volume ratio in Figure S5 and find a strong linear correlation between δ_{rt} and rod−rod distance. The definition of δ_{rt} is that when comparing two temperatures T_1 and T_2, $\delta_{rt} = \left(\frac{1}{T_1} - \frac{1}{T_2}\right)$. The analogous effects of the decreasing confinement size and lowering temperature imply that the hydrophobically confined water diffuses as if it was at a lower effective temperature, suggesting that one can gain insight into the confinement effect by studying the temperature dependence of water dynamics.

The Arrhenius plot for the diffusion coefficient of water in Figure 3b is nonlinear over the temperature range examined, signaling an expected variation of E_a with temperature. While the dependence of E_a on temperature is usually weak in a narrow temperature range around room temperature, we posit that the larger variation seen here might be connected with a change of the local environment due to the changing temperature.[39] Indeed, the non-Arrhenius behavior of molecular motions near the solid−liquid phase transition has been attributed to an increased association timescale and lengthscale between molecules.[41,62,63] We quantify the connection between the molecular environment experienced by water and the residence time of water around water in the next few sections, where we show that both a lowered temperature and/or a smaller confinement size can increase the residence time of water around water. We therefore propose that the associations among water molecules provide the origin of the observed retarded water dynamics under hydrophobic confinement.

Temperature-Dependent Associations between Water Molecules in the Bulk. We now examine the residence-time correlation function $S(t)$ between water molecules in bulk water with temperatures ranging between

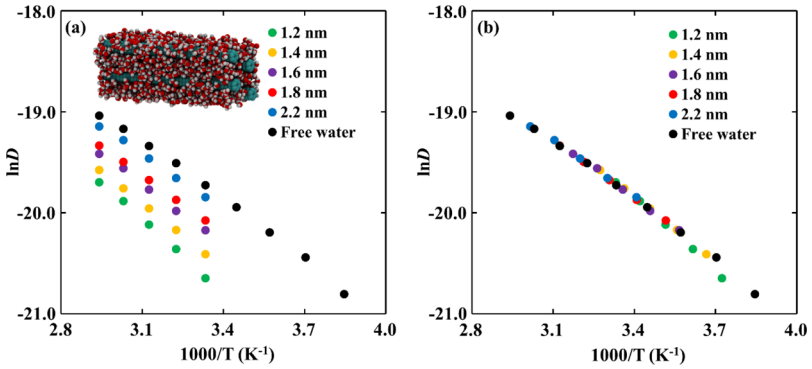

Figure 3. Arrhenius plots of ln D vs 1000/T for bulk and confined water in the rigid-rod model (the legend shows the rod−rod distance). Panel (a) represents the original data for diffusion coefficients at varying temperature. The temperature range is 300−340 K for confined water and 260−340 K for bulk water, both with 10 K intervals. Panel (b) represents the offset plots of the same data as in panel (a) such that there is an overlap between the confined and bulk water. The offset diffusion coefficients of confined water largely overlap those of free water, except the modest disagreement when the rod−rod distance is 1.2 nm.

https://doi.org/10.1021/acs.jpcb.1c06810
J. Phys. Chem. B 2021, 125, 13767−13777

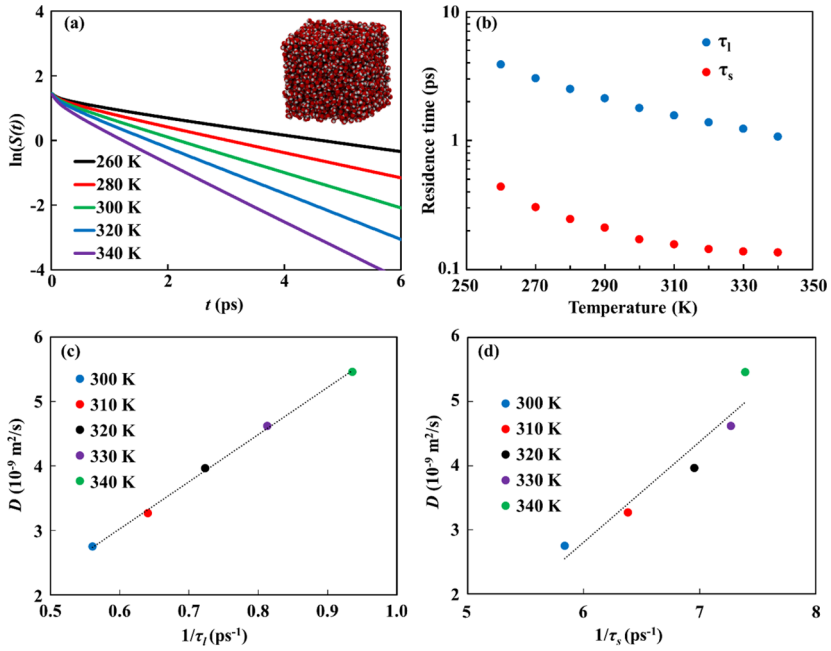

Figure 4. Panel (a) shows representative $\ln(S(t))$vs t plots generated from bulk water over a range of temperatures. The decay of $S(t)$ indicates loss of associations between neighboring water molecules. As temperature rises, the association lifetimes between adjacent molecules become increasingly short. Panel (b) shows the long and short residence times as a function of temperature. Both τ_s and τ_l show a monotonic decrease with the increasing temperature. The errors in τ_s and τ_l are estimated to be $\pm$0.02 and $\pm$0.05 ps, respectively. Panels (c) and (d) plot the diffusion coefficients of bulk water as a function of $1/\tau_l$ and $1/\tau_s$, respectively. The diffusion coefficients scale linearly with $1/\tau_l$, signaling a strong correlation between D and τ_l. The diffusion coefficients do not scale linearly with $1/\tau_s$, which supports that τ_s and τ_l carry different physical meanings.

260 and 340 K. Figure 4a shows $\ln(S(t))$ as a function of time at a few selected temperatures. We notice fast- and slow-decaying regions at short and long times, respectively, which can be nicely fitted with a double exponential decay model (see Methods). Figure 4b summarizes the numerical values of τ_s and τ_l extracted from the double exponential model, which quantify the residence times of the fast- and slow-decaying regions of the correlation function, respectively. Clearly, both residence times increase with decreasing temperature, implying that lowering the temperature prompts extended associations between water molecules in the bulk state.

When comparing the residence times of bulk water to the diffusion metrics D and E_a, longer residence times correlate with slower diffusion coefficients and higher activation energies. Intuitively, we argue that when longer timescale associations are at play, water molecules remain longer in the shell of their immediate neighbors, and diffusion becomes consequently slower. The lengthened associations between molecules are also responsible for the slowed molecular motions in supercooled liquids,[41,62] which agrees with what we observe here.

Further insight into the long and short residence times can be gained by visualizing the molecular motions on a picosecond timescale, where we notice two types of neighboring water molecules. One type of neighbor, corresponding to τ_l, resides relatively close to a central water molecule with which they associate for a relatively long period of time. Further analysis reveals that the diffusion coefficient, D, scales linearly with $1/\tau_l$ (Figure 4c), strongly suggesting a correlation between these two properties. The other type of neighbor, corresponding to τ_s, is on the edge of the cut-off distance, and these molecules experience interactions with the central molecule that quickly push them out of the solvation shell.

In this manuscript, we propose that these long and short residence times can be further understood in the context of the archetypal ballistic (inertial) and diffusive motions used to characterize bulk molecular motion.[25,64] On the timescale of picoseconds, the motion of water molecules transitions from ballistic to diffusive. Ballistic motion involves momentum-driven collisions with immediate neighboring molecules, while diffusive motion involves longer timescale evolution of the local solvation shell. Toward the end of τ_l, molecules are starting to disassociate from their initial neighbors or locally coordinated cage. Thus, τ_l indicates the timescale at which diffusive motions become dominant (we include a more in-depth analysis of the relation between D and τ_l in Figure S10). Contrary to the long residence-time behavior, the diffusion coefficients scale nonlinearly with $1/\tau_s$ (Figure 4d), which indicates that τ_s may report on a different metric of molecular dynamics from D. On the timescale of τ_s, the motions of molecules have not entered the diffusive regime and are therefore squarely in the pre-diffusive, ballistic stage.[25,65] In previous work, we noticed (based on NMR experiments and simulations) that the activation energy of diffusion, E_a, arises from molecular interactions and motions on a short picosecond timescale.[25,39] Thus, we propose that τ_s is correlated with E_a rather than with D, and we elaborate on this correlation in the later sections.

Water Associations in the Rigid-Rod Model. In the previous section, we quantified the effect of temperature on water dynamics by calculating the residence times over a range of temperatures for bulk water. In this section, we turn our attention to examining the dynamics of water molecules in a nanoconfined system using the same metrics. Figure 5 summarizes the residence time of water around water in the rigid-rod model. The residence time clearly increases with the decreasing rod−rod distance, which aligns with the parallelism

https://doi.org/10.1021/acs.jpcb.1c06810
J. Phys. Chem. B 2021, 125, 13767−13777

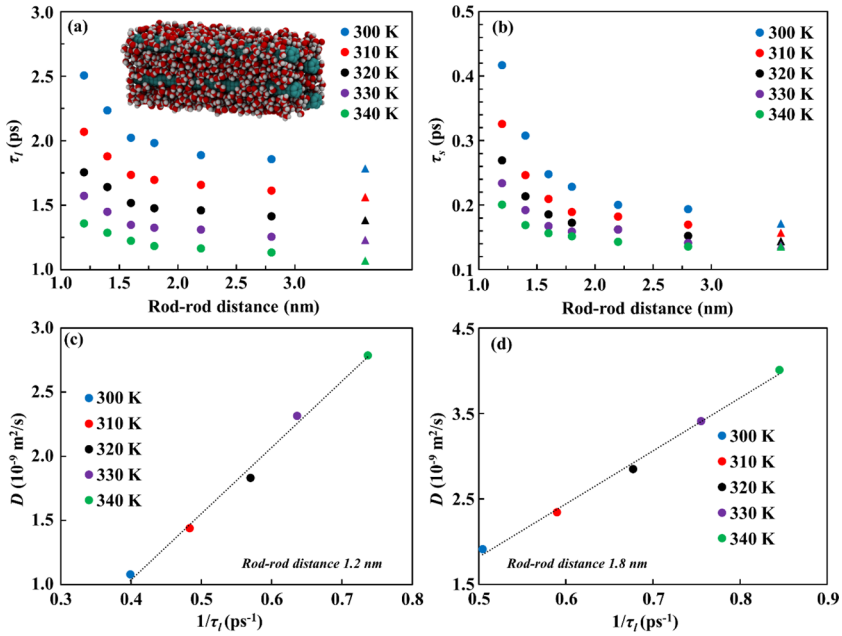

Figure 5. Panel (a) plots τ_l as a function of the rod−rod distance, while panel (b) plots τ_s as a function of the rod−rod distance for various temperatures. The residence time of confined water (circles) steadily decreases with the increasing rod−rod distance and converges to that of bulk water (triangles). Errors in τ_l and τ_s are estimated to be ±0.05 and ±0.02 ps, respectively. Panels (c) and (d) plot the diffusion coefficients of confined water as a function of $1/\tau_l$ for rod−rod distances of 1.2 and 1.8 nm, respectively. The linear relationship between D and $1/\tau_l$ remains valid for confined water.

between confinement and decreasing temperature revealed before. The trend in residence time of confined water supports the notion that nanoconfinement prompts longer associations between water molecules and furthers the concept that prolonged water associations are responsible for retarded water dynamics under rigid-rod confinement.

While the effects of reduced temperature and hydrophobic confinement on the residence time are similar, we believe the mechanisms behind the two effects are different. Lowering the temperature reduces thermal motion, limiting the energy available to a molecule to escape the shell of neighboring molecules. Hydrophobic nanoconfinement, on the other hand, physically limits the molecules' freedom of motion, resulting in more restrictions (in the direction of the confining wall) to escape their hydration shell and thus longer aggregations with their neighbors. In the rigid-rod model, highly retarded water dynamics become apparent at relatively small rod−rod distances (<1.6 nm) because the hydration shell of water, whose radius is similar to the 0.33 nm cut-off distance, is also small in size. Note that the rod−rod distance, which is the distance between the rod centers, is not the size of the confinement. Considering the excluded volume of the carbon atoms, the size of the water pocket in the rigid-rod model is around 0.8 nm at a rod−rod distance of 1.2 nm. Only when the confinement size is similar to the size of the hydration shell, the motions of the neighboring water molecules are limited enough that long-time aggregations become prominent.

The decrease in the value of τ_l with increasing rod−rod distance (Figure 5a) matches nicely the increase in diffusion coefficient in the same models (Figure 2c). Figure 5c,d plots the diffusion coefficients of confined water in this model with respect to $1/\tau_l$, and we observe a linear relationship reminiscent of that in bulk water (Figure 4c). On the other hand, the diffusion coefficients do not scale linearly with $1/\tau_s$ for confined water (see Figure 6a,b below), as in the case of bulk water (Figure 4d).

There are subtle differences in the variation of τ_s and τ_l with confinement size and temperature in Figure 5a,b that merit further discussion. First, the relative increase in τ_l with decreasing rod−rod distance is smaller than that of τ_s, which indicates that τ_s is more sensitive to the confinement size. As mentioned previously, τ_s originates from the dynamics of the outer-shell molecules, which rationalizes its larger dependence on the confinement size than the inner-shell motions responsible for τ_l. Second, the temperature dependence of τ_s is more sensitive to the rod−rod distance than that of τ_l. To quantify this temperature dependence, we calculated the E_a of the τ_s and τ_l residence times using an Arrhenius representation (shown in Figure 6c as a function of the rod−rod distance). The activation energy in the figure is obtained from an Arrhenius fit to the equation $\frac{1}{\tau} = \frac{1}{\tau_0} e^{-E_a/RT}$, so it can be interpreted as the activation energy of the residence rate constant. The variation of E_a of τ_s with rod−rod distance in Figure 6c is highly reminiscent of the variation of the activation energy of diffusion with rod−rod distance in Figure 2d. In fact, both activation energies do not change significantly in the 2−3 nm rod−rod distance range and then increase by less than 50% up to 1.2 nm. On the other hand, the E_a of τ_l shows variation with rod−rod distances beyond 2 nm, and it varies by a factor of 2.5 between 3 and 1.2 nm rod−rod distance. These observations further support that τ_s is much better correlated with E_a than τ_l. Figure 7 summarizes the current understanding of τ_l and τ_s based on the empirical correlations with the diffusion coefficient and activation energy of diffusion discussed in this work.

Water Associations in the Parallel-Sheet and Nanotube Models. We now discuss the dynamics of water confined between the two parallel graphene sheets. Within

https://doi.org/10.1021/acs.jpcb.1c06810
J. Phys. Chem. B 2021, 125, 13767−13777

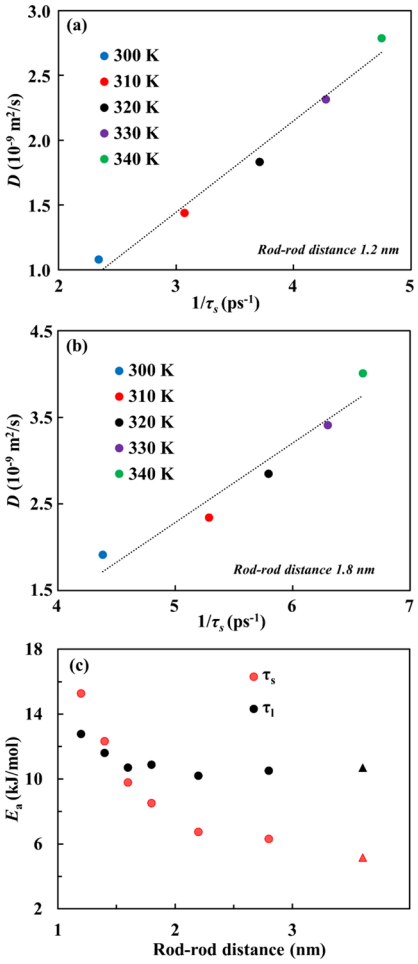

Figure 6. Panels (a, b) plot the diffusion coefficients of confined water in the rigid-rod model as a function of $1/\tau_s$ for 1.2 and 1.8 nm rod−rod distances, respectively. Similar to what is observed in bulk water, D is nonlinear with $1/\tau_s$. Panel (c) shows the Arrhenius activation energies (obtained from an Arrhenius fit to the equation $\frac{1}{\tau} = \frac{1}{\tau_0} e^{-E_a/RT}$) of the two residence times as a function of the rod−rod distance. For $1/\tau_l$, the temperature dependence drops slightly when the rod−rod distance increases from 1.2 to 1.6 nm but stays almost constant at the bulk-water value (triangle) at longer distances. For $1/\tau_s$, the temperature dependence decreases continuously toward the bulk-water value (triangle). When comparing the trends of the activation energy of $1/\tau_l$ and $1/\tau_s$ with rod−rod distance to that of E_a of diffusion (Figure 2d), the variation of E_a of $1/\tau_s$ matches that of E_a of diffusion, again suggesting a correlation of τ_s with E_a.

the confined region, the diffusion coefficient of water perpendicular to the sheets is zero. Thus, we only consider the water diffusion parallel to the graphene sheets. Figure 8a shows the Arrhenius plots of the diffusion coefficients of confined water in this model compared to bulk water. This parallel-sheet model also exhibits an increase of E_a with a smaller confinement size, reaching a maximum at a separation of 0.7 nm. Note that the temperature range for a layer-to-layer distance of 0.7 nm is different from the rest because at 300 and 310 K, we observe that water molecules form a partially ordered "squared ice" structure.[66,67] This structured water becomes disordered beyond 320 K, and we therefore have used a 320−360 K temperature range for these simulations. Figure 8b shows the τ_l of confined water in the parallel-sheet model. Much as with the diffusion coefficients and activation energies of diffusion, the residence time of confined water is slightly longer than that of bulk water at the largest layer-to-layer distance of 1.8 nm, signifying that confinement is active within that range.

In addition to the parallel-sheet model, we have also examined the water dynamics inside the CNTs. As previous work has shown, water molecules inside CNTs form a partially ordered structure when the tube diameter is close to 1.2 nm.[14,39] This ordering strongly slows down the water dynamics[38,39] and impairs quantification of diffusion metrics. Figure 8c shows the diffusion coefficients along the tube axis as a function of the tube diameter. While the dependence of diffusion coefficients on tube diameter is quite slight, we observe an increase in residence time with the decreasing tube diameters (Figure 8d), which however is much more moderate than in the other models.

An important emerging trend in our understanding of confined water is that regardless of the geometry of hydrophobic nanoconfinement, tighter confinement volumes prompt longer associations between water molecules. The prolonged water associations in turn justify the retarded water dynamics under nanoconfinement. As pointed out in the previous section, the local network of water molecules becomes more enduring when the confinement size is commensurate with the hydration shell (see Figure 9 for illustrations). Longer associations imply longer survival of the hydration shell and slower random diffusive motions. Furthermore, molecules moving more slowly have a greater propensity to sample the deepest regions of the intermolecular attractive potential well, leading to an increase in the effective energy barrier for diffusion.

Impact of Water−Surface Interactions on the Associations between Water Molecules. We now explore how the interaction potential between the atoms forming the confinement medium and water affects the dynamics of confined water. To shed light on this issue, we present the results for the 1.2 and 1.8 nm rigid-rod models in which the C-atom Lennard-Jones attraction well depths are 2 and 4 times greater than that in the original simulation (parameters shown in Table 1). The location of the potential well does not change from the original setup to isolate the effect of the interaction strength.

Figure 10 summarizes the results obtained with a rod−rod distance of 1.2 nm. Figure 10a,b shows the Arrhenius plots of water diffusion under the two modified force fields. As the water−rod attractions increase, the diffusion of water slows down and the activation energy increases slightly. Figure 10c plots the residence time of water around water comparing the modified and original force fields. Interestingly, the associations between water molecules increase when the water−rod interactions become stronger. Figure 10d plots the residence time of water around rods with a cut-off distance of 0.55 nm between the center of the rods and the O atom of the neighboring molecules, which captures the first solvation layer of the rods. Unsurprisingly, the water molecules become more associated with the rods with enhanced water−rod attractions. These results suggest that the increased carbon−water Lennard-Jones interactions act to anchor the water molecules within the surface layer of the rod. The residence time of water around those anchored surface waters consequently increases, justifying the results in Figure 10c. Additional calculations reveal that the increased associations between water molecules

https://doi.org/10.1021/acs.jpcb.1c06810
J. Phys. Chem. B 2021, 125, 13767−13777

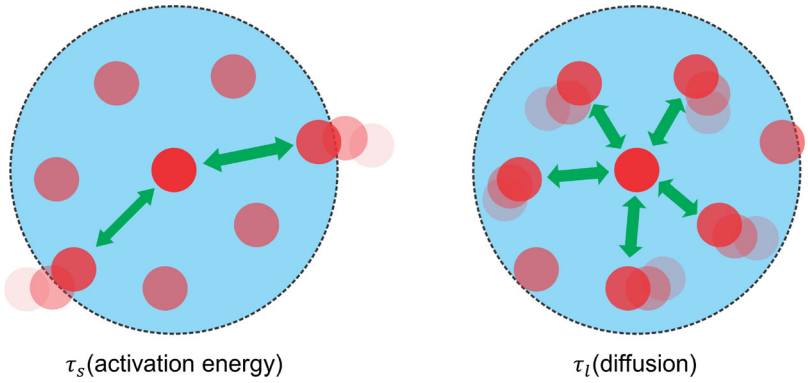

Figure 7. Illustrations of the molecular motions associated with τ_l and τ_s. On the one hand, τ_s originates from the interactions between a center molecule and molecules on the verge of leaving the cut-off distance (the dashed circle represents the cut-off). On the other hand, τ_l originates from the relatively more stable interactions between a center molecule and its immediate neighbors. As observed and discussed in the previous sections, τ_s correlates with the activation energy while τ_l correlates with the diffusion coefficient.

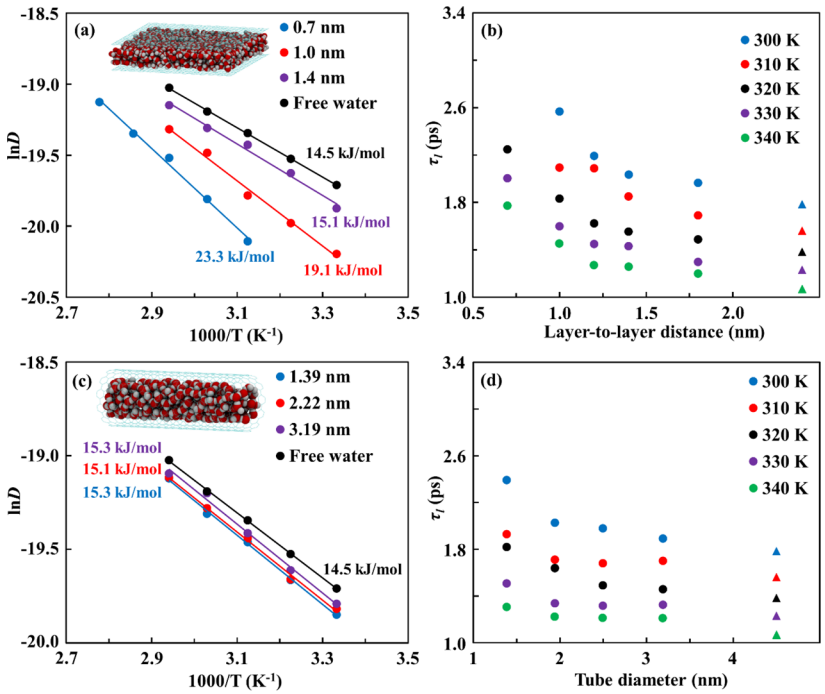

Figure 8. Panel (a) shows the Arrhenius plots of bulk and confined water in the parallel-sheet model as a function of layer-to-layer distance. Panel (b) shows the τ_l of confined water in the parallel-sheet model as a function of layer-to-layer distance. Panels (c, d) correspond to the Arrhenius plots and τ_l of water in the CNT model as a function of tube diameter. The triangles represent the residence times of bulk water.

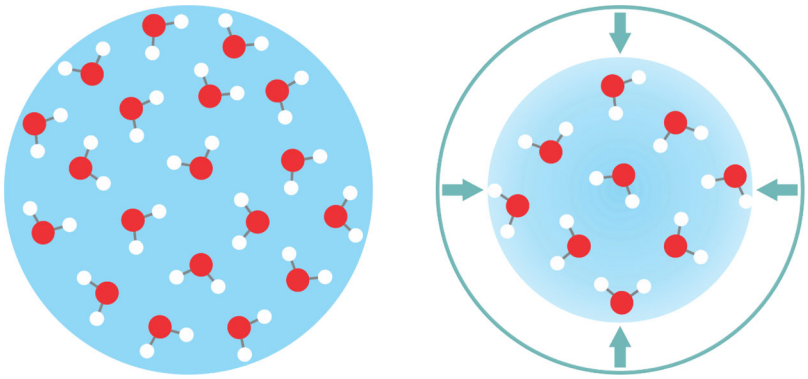

Figure 9. Schematic comparison of bulk water (left panel) and confined water (right panel). For confined water, an external boundary exists (shown as cyan circle). When the confinement size is similar to the size of the solvation shell, repulsion (shown as cyan arrows) from the confining surface limits the motions of water molecules, prompting longer associations between the neighboring molecules.

https://doi.org/10.1021/acs.jpcb.1c06810
J. Phys. Chem. B 2021, 125, 13767−13777

Table 1. Modified Lennard-Jones Parameters of Carbon Atoms in the Rigid-Rod Simulations

	σ_c (nm)	ε_c (kJ/mol)
original	0.355	0.293
model 1	0.355	0.586
model 2	0.355	1.172

are not exclusive to the small 1.2 nm rod−rod distance of Figure 10 but still persist at a rod−rod distance of 1.8 nm (Figure S11). Moreover, calculation of the residence time of water as a function of the distance from the rod (Table S2) shows that the increase of the carbon−water attractions mostly strengthens the associations of water molecules in the first surface layer while having a weaker impact on the water molecules more removed from the rods. Clearly, increasing the interactions between the confining medium surface and water causes retarded dynamics and slower diffusion, but these effects are relatively weak in comparison to the overall effect of geometric confinement.

CONCLUSIONS

The molecular dynamics simulations of this work reveal that hydrophobic confinement retards water motion as long as the confinement size is small enough (around 1 nm). Water molecules under hydrophobic confinement geometries (including CNTs, parallel sheets, and hexagonally packed rigid rods) diffuse effectively as if they were at a lower temperature and exhibit prolonged associations with the neighboring water molecules. Analysis of the residence-time correlation function of water around water demonstrates that residence times increase with either lowering temperature or decreasing confinement size. We argue that the associations between water molecules in the confined systems result from the physical restriction of the confinement medium, which limits the number of possible pathways for molecular motion. The associated molecular motions lower the diffusion coefficient and increase the activation energy of diffusion. The nanoconfinement effect becomes more prominent at smaller confinement sizes due to a direct impact on the hydration shell of water molecules.

We extract two residence times, τ_l and τ_s, from the calculations of residence-time correlation functions. Through visualization of molecular motions, we attribute τ_l to the inner-shell neighbors, which remain with a molecule for a relatively long period of time, and τ_s to the outer-shell neighbors, which experience short-lived collisions with the molecule and leave the vicinity of the central molecule more quickly. We observe that τ_s is more sensitive to the changing confinement size than τ_l. We also reveal that both τ_l and τ_s can be closely related to distinct water diffusion metrics. For instance, the inverse long residence time $(1/\tau_l)$ is linearly correlated with the diffusion coefficient in both bulk and confined water. However, the variation of the E_a of τ_s with confinement size mimics reasonably well the variation of the E_a of diffusion with confinement size, suggesting a relationship between τ_s and the activation energy of diffusion instead. Further investigation is needed to reveal the quantitative relations between E_a and τ_s.

Additional insight is provided via examination of the association between water molecules with changing water−surface Lennard-Jones interactions. Increased water−surface attraction localizes water molecules in the surface layer, resulting in modestly longer associations among water molecules and further slowdown of water dynamics.

Overall, we show that the residence time of water around water is strongly correlated with the diffusion behavior of water molecules, either in bulk or in confinement. We reveal increased residence time of water around water under various

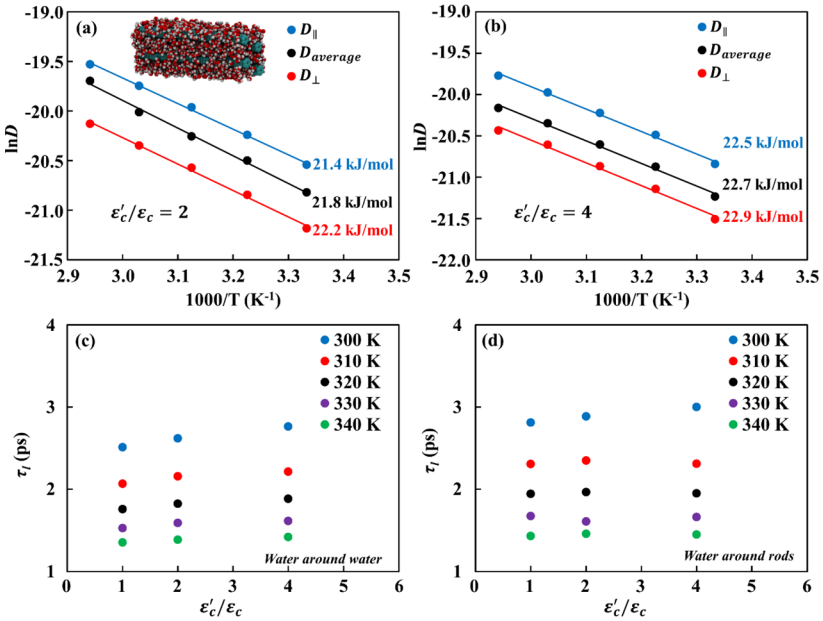

Figure 10. Impact of changing hydrophobicity on diffusion and residence times. Panels (a, b) present the Arrhenius plots of the diffusion coefficients of confined water in the rigid-rod models with a rod−rod distance of 1.2 nm and modified hydrophobicity. In panel (a), the modified Lennard-Jones parameter of the carbon atom (ε_c') is twice as strong as the original parameter (ε_c). In panel (b), ε_c' is four times as high as ε_c. Note that the average E_a with the original force field is 20.1 ± 0.1 kJ/mol (shown in Figure 2a). Panel (c) shows the τ_l of water around water comparing the original force fields and modified force fields. Panel (d) shows the τ_l of water around the rods comparing the original force fields and modified force fields. Somewhat surprisingly, the effects of substantially increasing the water−rod interactions (rod hydrophilicity) are relatively weak.

https://doi.org/10.1021/acs.jpcb.1c06810
J. Phys. Chem. B 2021, 125, 13767−13777

confining geometries, which prompts retarded water dynamics under hydrophobic confinement. Analysis of residence times therefore appears to be an attractive tool in the future characterization of diffusive behavior of mobile molecules in a variety of local environments.

■ ASSOCIATED CONTENT

Supporting Information

The Supporting Information is available free of charge at https://pubs.acs.org/doi/10.1021/acs.jpcb.1c06810.

Visualized snapshots of the simulation systems. Insights into the relationship between the diffusive activation energy and the front factor from the rigid-rod model. Comparison of activation energy vs confinement sizes across the various simulation models. The dependence of residence times on various factors including density, water model, and cut-off distance. Further insights into the physical meanings of the residence times (PDF)

■ AUTHOR INFORMATION

Corresponding Authors

Diego Troya − *Department of Chemistry and Macromolecules Innovation Institute, Virginia Tech, Blacksburg, Virginia 24061, United States;* orcid.org/0000-0003-4971-4998; Email: troya@vt.edu

Louis A. Madsen − *Department of Chemistry and Macromolecules Innovation Institute, Virginia Tech, Blacksburg, Virginia 24061, United States;* orcid.org/0000-0003-4588-5183; Email: lmadsen@vt.edu

Author

Rui Zhang − *Department of Chemistry and Macromolecules Innovation Institute, Virginia Tech, Blacksburg, Virginia 24061, United States*

Complete contact information is available at: https://pubs.acs.org/10.1021/acs.jpcb.1c06810

Notes

The authors declare no competing financial interest.

■ ACKNOWLEDGMENTS

This work was supported by the National Science Foundation under Awards DMR 1507764 and 1810194. Advanced Research Computing at Virginia Tech is gratefully acknowledged for providing computational resources and technical support that have contributed to the results reported within this paper.

■ REFERENCES

(1) Karaborni, S.; Smit, B.; Heidug, W.; Urai, J.; van Oort, E. The swelling of clays: Molecular simulations of the hydration of montmorillonite. *Science* **1996**, *271*, 1102−1104.

(2) Cailliez, F.; Trzpit, M.; Soulard, M.; Demachy, I.; Boutin, A.; Patarin, J.; Fuchs, A. H. Thermodynamics of water intrusion in nanoporous hydrophobic solids. *Phys. Chem. Chem. Phys.* **2008**, *10*, 4817−4826.

(3) Bordallo, H. N.; Aldridge, L. P.; Desmedt, A. Water dynamics in hardened ordinary Portland cement paste or concrete: From quasielastic neutron scattering. *J. Phys. Chem. B* **2006**, *110*, 17966−17976.

(4) Wang, Y.; He, Z.; Gupta, K. M.; Shi, Q.; Lu, R. Molecular dynamics study on water desalination through functionalized nanoporous graphene. *Carbon* **2017**, *116*, 120−127.

(5) Hummer, G.; Rasaiah, J. C.; Noworyta, J. P. Water conduction through the hydrophobic channel of a carbon nanotube. *Nature* **2001**, *414*, 188−190.

(6) Pratt, L. R.; Pohorille, A. Hydrophobic effects and modeling of biophysical aqueous solution interfaces. *Chem. Rev.* **2002**, *102*, 2671−2692.

(7) Luo, P.; Baldwin, R. L. Interaction between water and polar groups of the helix backbone: An important determinant of helix propensities. *PNAS* **1999**, *96*, 4930−4935.

(8) Israelachvili, J.; Wennerstrom, H. Role of hydration and water structure in biological and colloidal interactions. *Nature* **1996**, *379*, 219−225.

(9) Christenson, H. K. Confinement effects on freezing and melting. *J. Phys.: Condens. Matter* **2001**, *13*, R95−R133.

(10) Gelb, L. D.; Gubbins, K. E.; Radhakrishnan, R.; Sliwinska-Bartkowiak, M. Phase separation in confined systems. *Rep. Prog. Phys.* **1999**, *62*, 1573−1659.

(11) Zhang, J.; Liu, G.; Jonas, J. Effects of Confinement on the Glass-Transition Temperature of Molecular Liquids. *J. Phys. Chem.* **1992**, *96*, 3478−3480.

(12) Beckstein, O.; Sansom, M. S. P. Liquid-vapor oscillations of water in hydrophobic nanopores. *PNAS* **2003**, *100*, 7063−7068.

(13) Zaragoza, A.; Gonzalez, M. A.; Joly, L.; Lopez-Montero, I.; Canales, M. A.; Benavides, A. L.; Valeriani, C. Molecular dynamics study of nanoconfined TIP4P/2005 water: how confinement and temperature affect diffusion and viscosity. *Phys. Chem. Chem. Phys.* **2019**, *21*, 13653−13667.

(14) Mashl, R. J.; Joseph, S.; Aluru, N. R.; Jakobsson, E. Anomalously immobilized water: A new water phase induced by confinement in nanotubes. *Nano Lett.* **2003**, *3*, 589−592.

(15) Koga, K.; Gao, G. T.; Tanaka, H.; Zeng, X. C. Formation of ordered ice nanotubes inside carbon nanotubes. *Nature* **2001**, *412*, 802−805.

(16) Cicero, G.; Grossman, J. C.; Schwegler, E.; Gygi, F.; Galli, G. Water confined in nanotubes and between graphene sheets: A first principle study. *J. Am. Chem. Soc.* **2008**, *130*, 1871−1878.

(17) Holt, J. K.; Park, H. G.; Wang, Y. M.; Stadermann, M.; Artyukhin, A. B.; Grigoropoulos, C. P.; Noy, A.; Bakajin, O. Fast mass transport through sub-2-nanometer carbon nanotubes. *Science* **2006**, *312*, 1034−1037.

(18) Steudle, E.; Henzler, T. Water Channels in Plants - Do Basic Concepts of Water Transport Change. *J. Exp. Bot.* **1995**, *46*, 1067−1076.

(19) Horner, A.; Pohl, P. Single-file transport of water through membrane channels. *Faraday Discuss.* **2018**, *209*, 9−33.

(20) Mietner, J. B.; Brieler, F. J.; Lee, Y. J.; Froba, M. Properties of Water Confined in Periodic Mesoporous Organosilicas: Nano-imprinting the Local Structure. *Angew. Chem., Int. Ed.* **2017**, *56*, 12348−12351.

(21) Hou, D.; Li, D.; Zhao, T.; Li, Z. Confined Water Dissociation in Disordered Silicate Nanometer-Channels at Elevated Temperatures: Mechanism, Dynamics and Impact on Substrates. *Langmuir* **2016**, *32*, 4153−4168.

(22) Briman, I. M.; Rebiscoul, D.; Diat, O.; Zanotti, J. M.; Jollivet, P.; Barboux, P.; Gin, S. Impact of Pore Size and Pore Surface Composition on the Dynamics of Confined Water in Highly Ordered Porous Silica. *J. Phys. Chem. C* **2012**, *116*, 7021−7028.

(23) Sattig, M.; Reutter, S.; Fujara, F.; Werner, M.; Buntkowsky, G.; Vogel, M. NMR studies on the temperature-dependent dynamics of confined water. *Phys. Chem. Chem. Phys.* **2014**, *16*, 19229−19240.

(24) Manzano, H.; Moeini, S.; Marinelli, F.; van Duin, A. C. T.; Ulm, F. J.; Pellenq, R. J. M. Confined Water Dissociation in Microporous Defective Silicates: Mechanism, Dipole Distribution, and Impact on Substrate Properties. *J. Am. Chem. Soc.* **2012**, *134*, 2208−2215.

(25) Lingwood, M. D.; Zhang, Z.; Kidd, B. E.; McCreary, K. B.; Hou, J.; Madsen, L. A. Unraveling the local energetics of transport in a polymer ion conductor. *Chem. Commun.* **2013**, *49*, 4283−4285.

(26) Kidd, B. E.; Forbey, S. J.; Steuber, F. W.; Moore, R. B.; Madsen, L. A. Multiscale Lithium and Counterion Transport in an Electrospun Polymer-Gel Electrolyte. *Macromolecules* **2015**, *48*, 4481−4490.
(27) Thieu, L. M.; Zhu, L.; Korovich, A. G.; Hickner, M. A.; Madsen, L. A. Multiscale Tortuous Diffusion in Anion and Cation Exchange Membranes. *Macromolecules* **2019**, *52*, 24−35.
(28) Hou, J.; Li, J.; Madsen, L. A. Anisotropy and Transport in Poly(arylene ether sulfone) Hydrophilic-Hydrophobic Block Copolymers. *Macromolecules* **2010**, *43*, 347−353.
(29) Chang, K.; Korovich, A.; Xue, T.; Morris, W. A.; Madsen, L. A.; Geise, G. M. Influence of Rubbery versus Glassy Backbone Dynamics on Multiscale Transport in Polymer Membranes. *Macromolecules* **2018**, *51*, 9222−9233.
(30) Youssef, M.; Pellenq, R. J. M.; Yildiz, B. Glassy Nature of Water in an Ultraconfining Disordered Material: The Case of Calcium-Silicate-Hydrate. *J. Am. Chem. Soc.* **2011**, *133*, 2499−2510.
(31) Gallo, P.; Rovere, M.; Ricci, M. A.; Hartnig, C.; Spohr, E. Evidence of glassy behaviour of water molecules in confined states. *Philos. Mag. B* **1999**, *79*, 1923−1930.
(32) Major, R. C.; Houston, J. E.; McGrath, M. J.; Siepmann, J. I.; Zhu, X. Y. Viscous water meniscus under nanoconfinement. *Phys. Rev. Lett.* **2006**, *96*, 177803.
(33) Majumder, M.; Chopra, N.; Andrews, R.; Hinds, B. J. Nanoscale hydrodynamics: enhanced flow in carbon nanotubes. *Nature* **2005**, *438*, 44.
(34) Layfield, J. P.; Troya, D. Molecular simulations of the structure and dynamics of water confined between alkanethiol self-assembled monolayer plates. *J. Phys. Chem. B* **2011**, *115*, 4662−4670.
(35) Choudhury, N.; Pettitt, B. M. Dynamics of water trapped between hydrophobic solutes. *J. Phys. Chem. B* **2005**, *109*, 6422−6429.
(36) Choudhury, N. Orientational dynamics of water trapped between two nanoscopic hydrophobic solutes: A molecular dynamics simulation study. *J. Chem. Phys.* **2010**, *133*, 154515.
(37) Liu, Y. C.; Wang, Q.; Wu, T.; Zhang, L. Fluid structure and transport properties of water inside carbon nanotubes. *J. Chem. Phys.* **2005**, *123*, 234701.
(38) Farimani, A. B.; Aluru, N. R. Spatial Diffusion of Water in Carbon Nanotubes: From Fickian to Ballistic Motion. *J. Phys. Chem. B* **2011**, *115*, 12145−12149.
(39) Zhang, R.; Chen, Y.; Troya, D.; Madsen, L. A. Relating Geometric Nanoconfinement and Local Molecular Environment to Diffusion in Ionic Polymer Membranes. *Macromolecules* **2020**, *53*, 3296−3305.
(40) Watanabe, K.; Kawasaki, T.; Tanaka, H. Structural origin of enhanced slow dynamics near a wall in glass-forming systems. *Nat. Mater.* **2011**, *10*, 512−520.
(41) Bennemann, C.; Donati, C.; Baschnagel, J.; Glotzer, S. C. Growing range of correlated motion in a polymer melt on cooling towards the glass transition. *Nature* **1999**, *399*, 246−249.
(42) Hua, L.; Huang, X.; Zhou, R.; Berne, B. J. Dynamics of water confined in the interdomain region of a multidomain protein. *J. Phys. Chem. B* **2006**, *110*, 3704−3711.
(43) Horstmann, R.; Sanjon, E. P.; Drossel, B.; Vogel, M. Effects of confinement on supercooled tetrahedral liquids. *J. Chem. Phys.* **2019**, *150*, 214704.
(44) Li, J.; Park, J. K.; Moore, R. B.; Madsen, L. A. Linear coupling of alignment with transport in a polymer electrolyte membrane. *Nat. Mater.* **2011**, *10*, 507−511.
(45) Bates, C. M.; Bates, F. S. 50th Anniversary Perspective: Block Polymers—Pure Potential. *Macromolecules* **2017**, *50*, 3−22.
(46) Mitchell, J. B.; Geise, N. R.; Paterson, A. R.; Osti, N. C.; Sun, Y. Y. L.; Fleischmann, S.; Zhang, R.; Madsen, L. A.; Toney, M. F.; Jiang, D. E.; Kolesnikov, A. I.; Mamontov, E.; Augustyn, V. Confined Interlayer Water Promotes Structural Stability for High-Rate Electrochemical Proton Intercalation in Tungsten Oxide Hydrates. *ACS Energy Lett.* **2019**, *4*, 2805−2812.
(47) Wang, Y.; Chen, Y.; Gao, J. W.; Yoon, H. G.; Jin, L. Y.; Forsyth, M.; Dingemans, T. J.; Madsen, L. A. Highly Conductive and Thermally Stable Ion Gels with Tunable Anisotropy and Modulus. *Adv. Mater.* **2016**, *28*, 2571−2578.
(48) Yu, Z.; He, Y.; Wang, Y.; Madsen, L. A.; Qiao, R. Molecular Structure and Dynamics of Ionic Liquids in a Rigid-Rod Polyanion-Based Ion Gel. *Langmuir* **2017**, *33*, 322−331.
(49) Van Der Spoel, D.; Lindahl, E.; Hess, B.; Groenhof, G.; Mark, A. E.; Berendsen, H. J. GROMACS: fast, flexible, and free. *J. Comput. Chem.* **2005**, *26*, 1701−1718.
(50) Hess, B.; Kutzner, C.; van der Spoel, D.; Lindahl, E. GROMACS 4: Algorithms for Highly Efficient, Load-Balanced, and Scalable Molecular Simulation. *J. Chem. Theory Comput.* **2008**, *4*, 435−447.
(51) Berendsen, H. J. C.; Vanderspoel, D.; Vandrunen, R. Gromacs - a Message-Passing Parallel Molecular-Dynamics Implementation. *Comput. Phys. Commun.* **1995**, *91*, 43−56.
(52) Berendsen, H. J. C.; Grigera, J. R.; Straatsma, T. P. The Missing Term in Effective Pair Potentials. *J. Phys. Chem.* **1987**, *91*, 6269−6271.
(53) Abascal, J. L. F.; Vega, C. A general purpose model for the condensed phases of water: TIP4P/2005. *J. Chem. Phys.* **2005**, *123*, 234505.
(54) Einstein, A. On the theory of the Brownian Motion. *Ann. Phys.* **1906**, *19*, 371−381.
(55) Brunne, R. M.; Liepinsh, E.; Otting, G.; Wuthrich, K.; van Gunsteren, W. F. Hydration of proteins. A comparison of experimental residence times of water molecules solvating the bovine pancreatic trypsin inhibitor with theoretical model calculations. *J. Mol. Biol.* **1993**, *231*, 1040−1048.
(56) Ding, Y.; Hassanali, A. A.; Parrinello, M. Anomalous water diffusion in salt solutions. *PNAS* **2014**, *111*, 3310−3315.
(57) Li, T.; Hassanali, A. A.; Singer, S. J. Origin of slow relaxation following photoexcitation of W7 in myoglobin and the dynamics of its hydration layer. *J. Phys. Chem. B* **2008**, *112*, 16121−16134.
(58) Bizzarri, A. R.; Cannistraro, S. Molecular Dynamics of Water at the Protein−Solvent Interface. *J. Phys. Chem. B* **2002**, *106*, 6617−6633.
(59) Mogurampelly, S.; Keith, J. R.; Ganesan, V. Mechanisms Underlying Ion Transport in Polymerized Ionic Liquids. *J. Am. Chem. Soc.* **2017**, *139*, 9511−9514.
(60) Zhao, W.; Leroy, F.; Heggen, B.; Zahn, S.; Kirchner, B.; Balasubramanian, S.; Muller-Plathe, F. Are There Stable Ion-Pairs in Room-Temperature Ionic Liquids? Molecular Dynamics Simulations of 1-n-Butyl-3-methylimidazolium Hexafluorophosphate. *J. Am. Chem. Soc.* **2009**, *131*, 15825−15833.
(61) Makarov, V. A.; Andrews, B. K.; Smith, P. E.; Pettitt, B. M. Residence times of water molecules in the hydration sites of myoglobin. *Biophys. J.* **2000**, *79*, 2966−2974.
(62) Bauer, T.; Lunkenheimer, P.; Loidl, A. Cooperativity and the Freezing of Molecular Motion at the Glass Transition. *Phys. Rev. Lett.* **2013**, *111*, 225702.
(63) Crauste-Thibierge, C.; Brun, C.; Ladieu, F.; L'Hote, D.; Biroli, G.; Bouchaud, J. P. Evidence of Growing Spatial Correlations at the Glass Transition from Nonlinear Response Experiments. *Phys. Rev. Lett.* **2010**, *104*, 165703.
(64) Callaghan, P. *Translational Dynamics and Magnetic Resonance: Principles of Pulsed Gradient Spin Echo NMR*; Oxford University Press: New York, 2011, DOI: 10.1093/acprof:oso/9780199556984.001.0001.
(65) Chandler, D. *Introduction to Modern Statistical Mechanics*; Oxford University Press: New York, 1987.
(66) Algara-Siller, G.; Lehtinen, O.; Wang, F. C.; Nair, R. R.; Kaiser, U.; Wu, H. A.; Geim, A. K.; Grigorieva, I. V. Square ice in graphene nanocapillaries. *Nature* **2015**, *519*, 443−445.
(67) Singla, S.; Anim-Danso, E.; Islam, A. E.; Ngo, Y.; Kim, S. S.; Naik, R. R.; Dhinojwala, A. Insight on Structure of Water and Ice Next to Graphene Using Surface-Sensitive Spectroscopy. *ACS Nano* **2017**, *11*, 4899−4906.